Performance Comparison of Ultra-Miniature Diffraction Gratings with Lenses and Zone Plates

Leonidas Spinoulas[1]*, Oliver Cossairt[1], Aggelos K. Katsaggelos[1], Patrick R. Gill[2] and David G. Stork[2]

[1]*Northwestern University, 2145 Sheridan Road, Evanston, IL, 60208, USA*
[2]*Rambus Labs, 1050 Enterprise Way, Suite 700, Sunnyvale, California, 94089, USA*
leonidasspinoulas2015@u.northwestern.edu

Abstract: In this work, we compare the performance of previously proposed ultra-miniature diffraction gratings with ideal lenses and zone plates of similar structural characteristics. The analysis aims at understanding the differences of designs utilizing non-focusing gratings and the potential benefits of their use in computational imaging systems.

OCIS codes: 050.1950, 110.1758.

1. Introduction

A new class of ultra-miniature diffraction gratings has been recently proposed [1]. These gratings impose phase anti-symmetry on the incoming wavefront effectively producing optical nulls which enable them to exhibit relatively constant response across wavelengths as well as insensitivity to manufactured grating thickness [2]. Hardware verification of these tiny gratings (on the scale of μm) has also been performed [3]. Admittedly, the purpose of such designs is not high-resolution imaging but their size and low cost could open new frontiers for their use in endoscopy, medical sensing or machine inspection and surveillance. Additionally, their design could be optimized for specialized non-imaging applications (*e.g.*, QR-code reading, face detection) [3].

Unlike traditional optical elements, which aim at producing a small Point Spread Function (PSF) in order to focus the incoming radiation, these diffraction gratings purposely diffract the incoming light producing a wide PSF. However, the measured PSF has been demonstrated to retain high frequency information while remaining relatively unchanged for a wide range of incident angles of radiation [2, 3], effectively enabling computational calculation of the captured scene using a reconstruction algorithm. In this work, we analyze the imaging capabilities of sensors employing such gratings as compared to traditional optical elements (*e.g.*, Fresnel zone plates and refractive lenses).

2. Imaging System Modeling

The studied gratings have a very small aperture resulting in an effective depth of field ranging from roughly $1\,mm$ to infinity. We consider incoherent far field imaging such that each point in the captured scene produces a wavefront that diminishes to a plane wave of a different incident angle when reaching the grating. Thus, one can model the propagation using Fraunhofer diffraction. The plane wave then passes through the grating and propagates within a medium of a certain refraction index until it reaches the underlying sensor. Usage of a propagation medium beneath the grating is essential for the construction of an imaging system in such small scales and such propagation can be modeled using Fresnel diffraction.

We consider a sensor of size $300 \times 300\,\mu m^2$ consisting of 120×120 photodetectors of area $2.5 \times 2.5\,\mu m^2$ each. The propagation medium has a refractive index of $n = 1.51$ and height of $f = 155.8\,\mu m$. The grating is etched at the top surface of the medium in order to produce phase reversal (*i.e.*, phase delay of π) for a wavelength of $\lambda = 500\,nm$. The grating shares the same size as the sensor but exhibits finer resolution with 1797×1797 elements of surface area $0.167 \times 0.167\,\mu m^2$ each, while the aperture size of the actual diffraction pattern is $55\,\mu m$. The studied grating is shown on the left part of Figure 1. The grating has a spiral profile and phase-antisymmetry is imposed perpendicular to its curved arms. The presented cross-section does not correspond to a phase-antisymmetric plane but rather a diagonal of the presented pattern. Additional examples of designs exhibiting phase-antisymmetry can be found in [3].

We choose to compare the spiral design with two standard optical focusing elements, specifically, a Fresnel zone plate and a refractive singlet lens. Keeping the same aperture size and propagation medium described above, the design parameters for each optical element can be uniquely identified. Specifically, the focal length is dictated by the distance

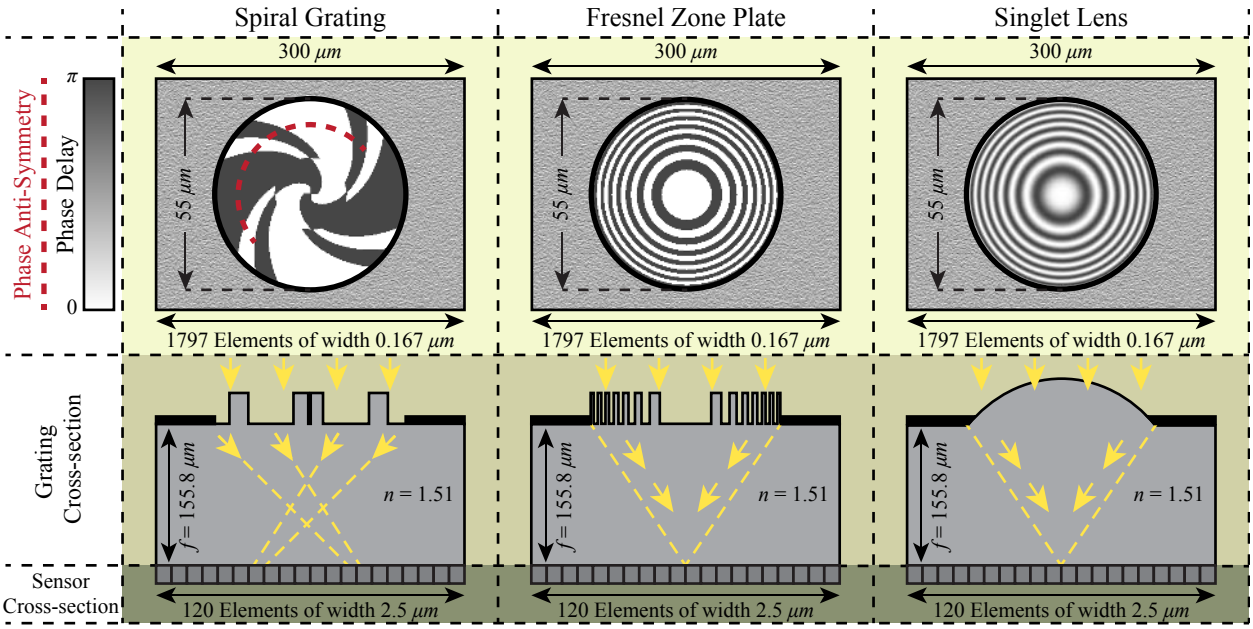

Fig. 1. Phase delay and structural characteristics for each one of the studied optical elements. All three elements were optimized for a wavelength of $\lambda = 500\,nm$ keeping the same aperture size, focal length (f) and refraction index (n) of the propagating medium. A phase delay of π is imposed by the gratings while the lens provides a continuous range of phase delays based on its curvature. Note that, phase delay color coding is to be understood as modulo π for the lens.

f from the grating to the sensor plane while the phase profile for each grating can be calculated using well known equations. The structural characteristics of each studied element are presented side to side in Figure 1.

3. Performance Comparison

We compare the three studied elements in terms of reconstruction quality for images covering a large range of incoming light angles (*i.e.*, field of view, FOV) adhering to the far field imaging assumption. Comparisons are conducted for a set of different wavelengths (remember that each element was optimized for $\lambda = 500\,nm$) and varying noise levels.

The signal acquisition procedure can be modeled as a linear operation,

$$\mathbf{y} = A\mathbf{x} + \mathbf{n}, \tag{1}$$

where each column of matrix $A : M \times N$ holds a vectorized version of the $m \times m = M$ diffraction response of the sensor for each one of N incoming radiation angles, $\mathbf{x} : N \times 1$ is the unknown image vector, $\mathbf{y} : M \times 1$ denotes the sensor measurements, while $\mathbf{n} : M \times 1$ represents noise. For our experiments, we consider an image of size 241×241 pixels corresponding to angles $(-60^o, 60^o)$, leading to $N = 241 \cdot 241$ and $M = 120 \cdot 120$, which is the considered sensor size.

Reconstruction is performed using a baseline algorithm, specifically, Tikhonov regularization,

$$\hat{\mathbf{x}} = \arg\min_{\mathbf{x}} \|\mathbf{y} - A\mathbf{x}\|_2^2 + \gamma\|\mathbf{x}\|_2^2, \tag{2}$$

where $\gamma > 0$ is a user specified regularization parameter related to the noise level. For realistic experiments, we further consider light falloff which is proportional to the $(cos\theta)^4$ term of the incoming light angle θ. Therefore, the original signal is first set to $\mathbf{x}_i \cdot (cos\theta_i)^4$ and the reconstructed signal is then corrected by $\hat{\mathbf{x}}_i/(cos\theta_i)^4$ for $i = 1 \cdots N$.

We perform experiments for wavelengths of 400, 500 and 600 nm and increasing levels of shot-noise (Poisson noise) and report the performance in terms of Peak Signal-to-Noise Ratio (PSNR) in Figure 2. For each experiment, a set of γ values centered around the noise variance level were tested and the best results are reported. Examples of corresponding measurements and reconstructed images are depicted in Figure 3.

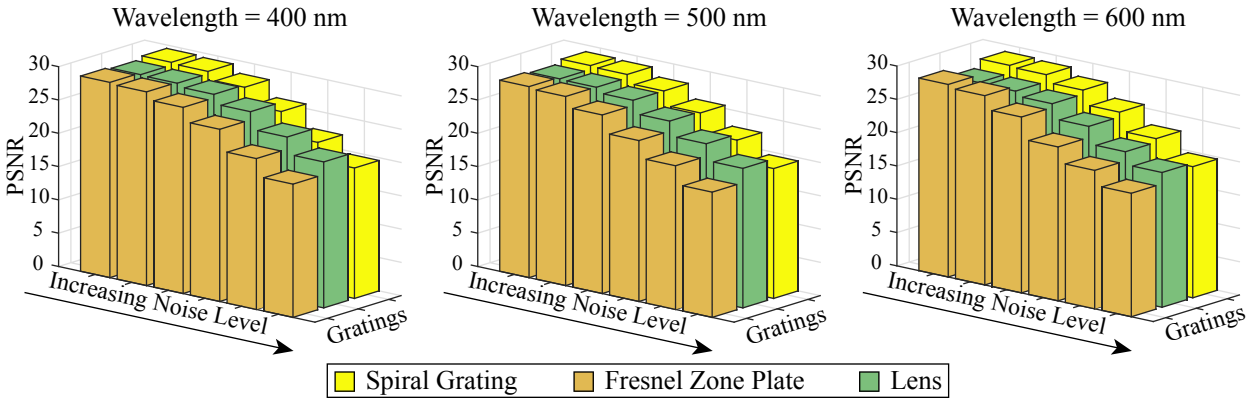

Fig. 2. Reconstruction performance comparison solving the problem in (2), for different incoming light wavelengths and various noise levels for all studied optical elements, presented in Figure 1.

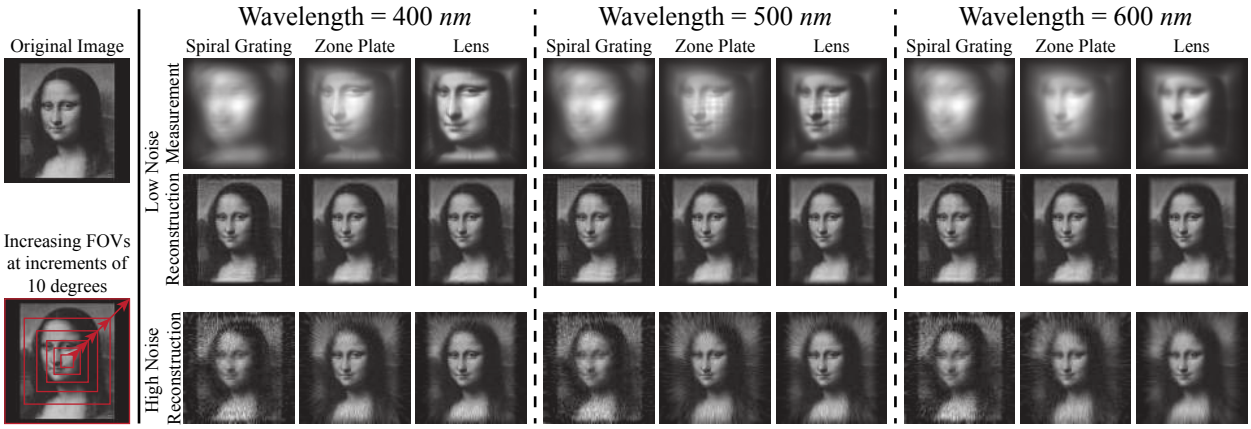

Fig. 3. Reconstructed images by solving the problem in (2), for different incoming light wavelengths and various noise levels for all studied optical elements, presented in Figure 1.

Figure 2 documents that reconstruction performance of the spiral gratings is consistent across wavelengths and compares favorably with the performance of the conventional "ideal" optical elements. Wavelength independence can also be observed by the sensor measurements for different wavelengths in Figure 3. In terms of image quality, a main difference that arises is that zone plates and lenses exhibit radially varying performance based on the incoming light angle. For the central part of the scene, reconstruction is nearly optimal while edges at the limits are severely blurred or corrupted with noise. Instead, the spiral grating exhibits a uniform reconstruction quality, being able to resolve high frequencies for large FOVs at the cost of lower image quality at small FOVs. The apparent ringing artifacts at high angles (please zoom-in) could be avoided by using a more sophisticated, edge-preserving, reconstruction technique. Finally, note that the tiny scale of the imager makes it challenging to fabricate and prone to manufacturing defects, under which, lenses and zone plates can produce great deviations from their optimal PSFs. Instead, the spiral grating, exhibiting good performance at varying depths of field [2, 3], could efficiently combat such imperfections.

References

1. P. R. Gill and D. G. Stork, "Lensless ultra-miniature imagers using odd-symmetry spiral phase gratings," in *Imaging and Applied Optics*, p. CW4C.3, Optical Society of America, 2013.
2. P. R. Gill, "Odd-symmetry phase gratings produce optical nulls uniquely insensitive to wavelength and depth," *Opt. Lett.*, vol. 38, pp. 2074–2076, Jun 2013.
3. D. G. Stork and P. R. Gill, "Optical, mathematical, and computational foundations of lensless ultra-miniature diffractive imagers and sensors," *International Journal on Advances in Systems and Measurements*, vol. 7, no. 3,4, pp. 201–208, 2014.